Numerical models of P–T, time and grain-size controls on Ar diffusion in biotite: an aide to interpreting $^{40}Ar/^{39}Ar$ ages

D.R. Skipton[a], C.J. Warren[b], F. Hanke[c]

[a]*Geological Survey of Canada, Natural Resources Canada, Ottawa, Ontario, K1A 0E8, Canada*

[b]*School of Environment, Earth and Ecosystem Sciences, The Open University, Walton Hall, Milton Keynes, MK7 6AA, United Kingdom*

[c]*Dassault Systèmes BIOVIA, 334 Science Park, Cambridge, CB4 0WN, United Kingdom*

This is a pre-print of a manuscript that has been submitted Chemical Geology.

Abstract

$^{40}Ar/^{39}Ar$ dating of biotite is used extensively to determine the timing of cooling and exhumation in metamorphic terranes. $^{40}Ar/^{39}Ar$ age interpretations commonly assume that ^{40}Ar diffuses out of biotite through temperature-dependent volume diffusion, and therefore that the age represents the time at which biotite cooled through the nominal closure temperature. Several processes or scenarios affect the reliability of the interpretation of $^{40}Ar/^{39}Ar$ ages as representing the timing of cooling through a nominal closure temperature, including incomplete re-setting of Ar systematics, incorporation of excess Ar, crystal defects acting as Ar traps or fast-pathways, or fluid-present recrystallization/dissolution. We present a series of numerical diffusion model results that show the percentage of radiogenic Ar that should theoretically be retained in biotite with different grain radii residing for various periods over a range of P–T conditions in a perfect open system that loses Ar via volume diffusion alone. A second set of models demonstrate the effects of crustal residence temperatures, residence timescales, and subsequent cooling rates, on 'perfect open system' biotite $^{40}Ar/^{39}Ar$ age and intra-grain Ar distributions. The model results are

useful for constraining cooling and exhumation histories from $^{40}Ar/^{39}Ar$ biotite data in a variety of metamorphic settings. They also provide baseline data for biotite Ar retention, $^{40}Ar/^{39}Ar$ ages and intra-grain age distributions that would theoretically be produced from volume diffusion acting alone. Consequently, the models can help evaluate the plausibility of alternative scenarios that may have affected biotite $^{40}Ar/^{39}Ar$ ages, including extraneous Ar contamination or Ar loss via processes other than diffusion. In conjunction with well-constrained petrogenetic histories, numerical diffusion models are a powerful tool for interpreting $^{40}Ar/^{39}Ar$ biotite ages, especially when linked with intra-grain $^{40}Ar/^{39}Ar$ age profiles.

Keywords

$^{40}Ar/^{39}Ar$ thermochronology, biotite, diffusion, numerical model, pressure-temperature, crustal residence

1. Introduction

^{40}Ar is produced from radioactive decay of ^{40}K, and has been shown to diffuse efficiently in biotite at temperatures above ~300°C (Harrison et al., 1985; McDougall and Harrison, 1999). It is assumed that Ar strongly partitions from minerals into the grain boundary (fluid-bearing) network, consistent with open-system behaviour (e.g., Kelley, 2002). Therefore, $^{40}Ar/^{39}Ar$ 'dates' yielded by biotite are typically assumed to relate to temperature-dependent diffusional Ar loss and thus constrain the timing of cooling following metamorphism. $^{40}Ar/^{39}Ar$ dating of biotite has been used for decades to constrain the timing of cooling, exhumation and low-temperature geological events worldwide (e.g., Berger, 1975; Hanson et al., 1975; Steltenpohl et al., 1993; Hodges and Bowring, 1995; McDougall and Harrison, 1999; Schneider et al., 1999, 2013; Willigers et al., 2001). For detailed discussion and calculations of Ar diffusion in biotite and the closure temperature concept, we refer the reader to previous studies (Dodson, 1973, 1986; Harrison et al., 1985; Wheeler, 1996; McDougall and Harrison, 1999).

Several studies have identified complexities of ^{40}Ar concentration in mica that call into question traditional interpretations of metamorphic $^{40}Ar/^{39}Ar$ ages as resulting solely from temperature-controlled volume diffusion (Heizler and Harrison, 1988; Lee, 1995; Kelley, 2002; Villa, 2010; Warren et al., 2011; Camacho et al., 2012; Cossette et al., 2015; Stübner et al., 2017). These studies suggest that alternative processes or scenarios affected the ^{40}Ar concentrations in biotite. $^{40}Ar/^{39}Ar$ dates that are older than the timing of cooling through the nominal closure temperature of ^{40}Ar (T_c) can be produced by: (i) incomplete re-setting of mica during metamorphism, resulting in retention of “inherited” (pre-thermal peak) ^{40}Ar (Warren et al., 2012a); (ii) incorporation and retention of excess Ar, which refers to parentless ^{40}Ar that is incorporated in the grain via diffusion from an Ar-rich grain boundary fluid network or contained within mineral/fluid inclusions (Kelley, 2002); (iii) planar defects in the crystal structure serving as ^{40}Ar traps (proposed in trioctohedral mica; Camacho et al., 2012); or (iv) recrystallization in a closed Ar-rich system, adding ^{40}Ar to grain rims (Warren et al., 2011). $^{40}Ar/^{39}Ar$ dates that are younger than the age of cooling through the nominal T_c can result from: (i) crystallization of the grain at or below the nominal T_c (e.g., Warren et al. 2012); (ii) planar defects in the crystal structure, such as those produced during deformation, serving as fast-pathways through which ^{40}Ar can escape (Lee, 1995; Hodges and Bowring, 1995); and (iii) isotopic resetting (^{40}Ar loss) due to fluid-present retrograde reactions / recrystallization / dissolution (Villa, 2010).

Metamorphic biotite is infamous for yielding $^{40}Ar/^{39}Ar$ ages that are older than those expected from volume diffusion during residence at high temperatures or cooling through the nominal ^{40}Ar T_c. Despite the higher nominal Ar T_c for muscovite (~420–450°C; Harrison et al., 2009), biotite in some cases yields $^{40}Ar/^{39}Ar$ dates that are substantially older than those of muscovite from the same rock, and may also pre-date U/Pb ages of metamorphic monazite or zircon. Such age relationships have been documented in several orogens, including the Paleoproterozoic Trans-Hudson (Skipton et al., 2017), Mesoproterozoic Grenville (Dallmeyer and Rivers, 1983; Cosca et al., 1991; Smith et al., 1994), Neoproterozoic Capricorn (Occhipinti and Reddy, 2009), Mesozoic Alpine (Brewer, 1969; Pickles et al., 1997) and Himalaya (Mottram et al., 2015; Stübner et al., 2017).

In the event that biotite yields an $^{40}Ar/^{39}Ar$ date that defies independent geological or isotopic evidence, the anomalous $^{40}Ar/^{39}Ar$ ratio is typically attributed to processes other than (or in addition to) volume diffusion, involving inherited or excess ^{40}Ar, crystal defects, recrystallization, dissolution, as described above, or dehydroxylation during vacuum heating (Harrison et al., 1985; Gaber et al., 1988; McDougall and Harrison, 1999). The degree of potential interpretational inaccuracy in such biotite ages is difficult to quantify, especially without models of Ar retention for different biotite radii and P–T histories. This has resulted in non-uniform interpretations of biotite $^{40}Ar/^{39}Ar$ data – which may be arbitrary without conclusive evidence for the process being invoked – and a general distrust and avoidance of biotite $^{40}Ar/^{39}Ar$ ages in recent metamorphic studies.

Here we present numerical models for volume diffusive loss of ^{40}Ar out of biotite over a range of geologically relevant temperatures (200–650°C) and pressures (0–2 GPa), and for different grain radii (0.1–5 mm) and residence times (1–1000 Myr). These models provide a baseline for ideal ^{40}Ar diffusion behaviour in biotite, according to experimentally established diffusion parameters, and demonstrate theoretical ^{40}Ar retentivity for various P–T scenarios to help interpret cooling/exhumation histories. Our models also enable comparisons with equivalent models for muscovite (Warren et al., 2012a) to aid age interpretations of co-existing biotite and muscovite. The calculated percentage of ^{40}Ar retention in biotite that would be expected from volume diffusion acting alone provides constraints on whether or not alternative processes may have affected the sample ^{40}Ar/^{39}Ar age. The models illustrate the significance of grain size, P–T and crustal residence time on ^{40}Ar diffusion, and demonstrate that excess Ar or changes to mica structure do not necessarily have to be invoked to explain ^{40}Ar/^{39}Ar ages that seem to conflict with other geochronometers. Our models also help to rule-in or rule-out certain scenarios, such as whether or not an ^{40}Ar/^{39}Ar age could reflect the timing of biotite growth, or the retention of pre-thermal peak radiogenic ^{40}Ar. Ar loss via dissolution-recrystallization would be faster than via diffusion, and assessing Ar retentivity as a function of temperature in biotite affected by dissolution-recrystallization would be invalid (Villa, 2010). Our models still apply in these cases, but only if the initial ("starting") temperature of the model is taken to be the temperature of recrystallization.

2. Methodology: numerical modeling of ^{40}Ar diffusion in biotite

Numerical models of ^{40}Ar diffusion in biotite were run using the MATLAB™ program DiffArgP (Wheeler, 1996; Warren et al., 2012a). The following parameters were used for the models (excluding uncertainties): activation energy (E_a) = 47 ± 2 kcal mol^{-1} (196 648 J mol^{-1}; Harrison et al., 1985); diffusion coefficient (D_0) = 0.077 $\frac{+0.21}{-0.06}$ cm^2 s^{-1} (Harrison et al., 1985); and activation volume (V_{act}) = 14 cm^3 mol^{-1} (Harrison et al., 1985; Grove and Harrison, 1996; Harrison et al., 2009). Harrison et al. (1985) indicate a 1σ uncertainty of ± ~0.1 log(D) units for diffusion coefficients calculated from experimental data. Including this uncertainty produced no significant difference to our model results.

The models were run using a cylindrical geometry because diffusive Ar loss in mica mainly occurs through in-plane diffusion in the crystal, which is typically modeled using cylindrical symmetry (Hames and Bowring, 1994). There has been some debate about the detailed geometry used to model these systems, but detailed analysis of diffusion coefficients has shown that the symmetry effects (e.g. cylindrical vs. spherical) on the diffusion coefficients can be expected to be substantially smaller than the measurement uncertainties listed above (Forster and Lister 2014). A Crank-Nicholson solver was used for the time integration with a time step that is 10 times larger than that required for the fully explicit model (following Wheeler, 1996; Warren et al., 2012a). It was assumed that volume diffusion occurred in an open system where the Ar concentration at the grain boundary was negligible (i.e., no excess ^{40}Ar in the grain boundary network) and the grain radius was equivalent to the diffusion radius. Numerical accuracy on the bulk ages was achieved following the methods outlined in Warren et al. (2012a, b). Representative model output data (integrated or "bulk" ^{40}Ar/^{39}Ar age for each model and a core-to-rim ^{40}Ar/^{39}Ar age profile), bulk age regression plots, and core-to-rim age profiles are shown in Supplementary File 1.

Models were run for a range of biotite grain radii (0.1, 0.5, 1, 2 and 5 mm) that are representative of the grain sizes typically analyzed for ^{40}Ar/^{39}Ar thermochronology. The models simulated residence times at peak conditions of 1, 5 and 20 Myr, which appear to be characteristic residence timescales for metamorphism in both modern and ancient orogens (e.g., 1–10 Myr, ca. 470 Ma Grampian Orogen, Scotland, Viete et al., 2011; 20–40 Myr, ca. 1830 Ma Trans-Hudson Orogen, Canada, Skipton et al., 2016; ≤1–5 Myr, ca. 10.5–21 Ma Sikkim Himalaya, Mottram et al., 2015). Residence times of 100, 500 and 1000 Myr were also modeled for grain radii of 0.1 to 1 mm to illustrate how Ar retention might be affected by long-term crustal residence such as expected / considered likely in Precambrian orogens. Coarser grain sizes were not considered because the high expected volumes of ^{40}Ar given their age are inhibitive for $^{40}Ar/^{39}Ar$ analyses. For a given biotite grain radius and residence time, models were run for a range of temperatures at 10°C increments to cover the full spectrum of Ar retentivity from 0% (complete ^{40}Ar loss) to 100% (all ^{40}Ar retained). Models were run using a pressure of 0.5 GPa; Ar retention at different pressures (0–2 GPa) was calculated using established values of E_a, P_0 and V_{act} (above) to map out equivalent diffusion coefficients across the entire pressure range. These model results were used to construct P–T diagrams showing %Ar retention in biotite for temperatures of 200–650°C and pressures up to 2 GPa (Figs. 1–3).

A second set of models was run to simulate the effect of various cooling/exhumation histories on Ar retention in 0.5 mm radius biotite (Figs. 4–6). For these models, biotite was first maintained at a temperature of 250°C, 350°C or 450°C and pressure of 0.7 GPa for different residence times (1, 20, 100, 500 or 1000 Myr). These conditions correspond to the red, blue and intermediate zones in the P-T-retention plots in Figs. 1–3. Following the defined residence periods, the modeled biotite was cooled at rates of 1.5, 10 or 30°C/Myr, which are representative cooling rates documented/suggested in Proterozoic and modern orogens (e.g., Dunlap, 2000). Decompression was modelled linearly with cooling, such that 0°C and 0 GPa were attained simultaneously in each model. A start time of 1500 Ma was used for this set of models to present all the modeled residence periods, temperatures and cooling rates from a common point in time, enabling straightforward comparison between models results shown in Figs. 4–6. The start time is otherwise arbitrary; the key detail is the amount of time that went unrecorded in the mica due to low Ar retentivity, i.e., the difference between the time at which the model started and the bulk age calculated by DiffArgP. In effect, the models can be applied to any period of geological interest.

3. Model results and interpretation

3.1. Plots of pressure–temperature–%Ar retention

Model results are shown on pressure–temperature plots with colour shading corresponding to percentages of ^{40}Ar retention (Figs. 1–3). As with equivalent models constructed for muscovite (Warren et al., 2012a), the blue zones represent P–T conditions of low Ar retention, the red zones represent conditions of high Ar retention, and orange-to-light blue zones reflect conditions of intermediate or partial Ar retention. Biotite that crystallized in or experienced peak metamorphism in the blue P–T zones would not theoretically retain any pre-thermal peak (inherited) radiogenic Ar. It is therefore capable of constraining the timing of cooling and exhumation. Due to high Ar retention in the red P–T zones, the $^{40}Ar/^{39}Ar$ age of biotite that crystallized at these conditions should, in an ideal system, reflect the timing of crystallization. Biotite that crystallised at lower conditions and subsequently experienced peak metamorphism in the red P–T zones would not have had the opportunity to lose its inherited (pre-thermal peak) ^{40}Ar before cooling initiated. Even if such a grain lost some Ar during cooling, it would still yield an older $^{40}Ar/^{39}Ar$ date than a grain that had crystallised at peak conditions, potentially resulting in overestimation of interpreted cooling rates. An $^{40}Ar/^{39}Ar$ age of biotite that crystallized in or experienced peak metamorphism in the "intermediate" P–T zones must also be interpreted with caution due to incomplete pre-peak degassing of ^{40}Ar.

The plots illustrate the significant dependence of ^{40}Ar retentivity on grain size and residence time, even for relatively short residence times of 1–20 Myr (Figs. 1, 2). For a given set of crustal residence conditions (temperature, pressure, time) within the intermediate zone, a 0.1 mm-radius grain is ~35% less retentive of Ar than a 1 mm-radius grain, which is ~25% less retentive than a 5 mm-radius biotite. For a biotite grain with a given radius residing at fixed P–T conditions in the intermediate zone, a grain residing for 20 Myr is ~35% less retentive than biotite residing for 1 Myr.

The plots simulating long-term crustal residence of 100–1000 Myr demonstrate the effects of geologic time on ^{40}Ar concentrations in biotite, especially in Precambrian orogens (Fig. 3). For a 1 mm-radius biotite, Ar retentivity is ~20, 40 or 60% lower for residence times of 100, 500 or 1000 Myr, respectively, compared to residence of 20 Myr. Time exerts the most extreme effects on Ar systematics in fine-grained, 0.1 mm-radius biotite: during 1 Ga residence at upper-crustal conditions of 250°C ($<T_c$) and $P \leq 0.5$ GPa, models suggest that the grain would lose at least ~50% radiogenic Ar through diffusion (Fig. 3i) before exhumation starts.

3.2. Models of cooling and exhumation histories for 0.5 mm radius biotite

Model results are shown as core-to-rim ^{40}Ar/^{39}Ar age profiles with corresponding bulk ages, calculated using a model start time of 1500 Ma (Figs. 4–6). For models in which biotite resided at 250°C for 1–100 Myr prior to cooling, bulk ages are ≤1 Myr younger than the onset of crustal residence (i.e., the model start time), and core-to-rim age profiles are relatively flat regardless of cooling rate (Figs. 4a–b, 5a). These model results reflect insignificant Ar diffusion in biotite at 250°C, as expected so far below the nominal T_c. For residence times of 500 Myr and 1 Gyr at 250°C, modelled core-to-rim age profiles exhibit diffusive Ar loss at outer grain edges and yield significantly lower bulk ages that are 28–30 Myr and 81–84 Myr, respectively, younger than the onset of crustal residence (Figs. 5b, 6a). This implies that low-temperature Ar ‘leakage’ from the outermost ≤50 μm of grain edges may be possible during long-term crustal residence of 0.5 mm-radius biotite in Precambrian orogens, and may affect $^{40}Ar/^{39}Ar$ step-heating or total fusion ages beyond analytical uncertainty.

For models in which biotite crystallised and resided at relatively cool temperatures of 350°C for various periods prior to cooling, slower cooling rates produce younger bulk ages and greater core-to-rim age decreases than those produced by faster cooling rates. This relationship reflects relatively efficient Ar diffusion at 350°C, which is more pronounced in grains that remained hotter for longer and/or that cooled more slowly. For a residence time of 1 Myr at 350°C, model ages are up to 10 Myr younger than the time of the onset of cooling below 350°C in each model. However, for all other residence periods modeled (20 Myr to 1 Gyr), resultant ages are older than the onset of cooling or, in the case of cooling at 1.5°C after 20 Myr residence, only 4 Myr younger than the onset of cooling. Therefore, these models illustrate the possible partial retention of ^{40}Ar in biotite during residence within the 'intermediate' P–T zone, and the importance of knowing the P–T conditions of biotite growth as well as its subsequent P–T path for interpreting the measured $^{40}Ar/^{39}Ar$ date.

Models of biotite crystallising then residing at higher temperatures (e.g., 450°C) for various periods followed by cooling at different rates all yielded ages younger than the time of onset of cooling, in accordance with highly efficient ^{40}Ar diffusion at 450°C. The slower the cooling rate, the younger the bulk age and the steeper the core-to-rim age profile, with all ages younger than those of equivalent models run with 350°C residence conditions. This is consistent with sustained diffusion of ^{40}Ar out of biotite that remains hotter than T_c for longer. Notably, for residence periods of 20 Myr and longer, core-to-rim age profile slopes of the 350°C models are steeper than those of 450°C models with equivalent cooling rates. This is inferred to reflect the less efficient diffusion of Ar at 350°C, hindering transport of Ar from the grain cores to the grain rims. Conversely, biotite residing at 450°C would experience more efficient Ar loss, such that the core-to-rim age gradient is controlled solely by the subsequent cooling rate. This is supported by our 450°C models: each cooling rate produced a distinct core-to-rim age gradient that is unaffected by residence time or when cooling began.

4. Discussion

4.1. Applicability of experimentally-determined Ar diffusion parameters to natural samples

Few studies have successfully conducted experimental measurements of ^{40}Ar diffusivity in biotite, in part due to the difficulty of maintaining the stability of hydroxyl-bearing minerals over the necessary temperature range. Harrison et al. (1985) addressed this issue by measuring radiogenic ^{40}Ar loss from biotite samples after hydrothermal-isothermal treatment; for each temperature run, biotite was heated at constant temperature in the presence of water to help maintain the mineral's stability. The biotite samples were ~56% annite, with radii of 56–202 μm, typical of biotite in granite and in most metamorphic rocks dated using $^{40}Ar/^{39}Ar$ (e.g., meta-granite, pelite, psammite). Equivalent experiments conducted on biotite richer in Fe provided nearly identical diffusion parameters (Grove and Harrison, 1996). For these reasons, in the absence of other reliable experimental values, and in consistency with most interpretations of $^{40}Ar/^{39}Ar$ biotite data we used the E_a and D_0 of Harrison et al. (1985) here (a comprehensive review is provided by McDougall and Harrison, 1999).

It has been argued that lab-measured diffusivities of hydrous minerals (biotite, phlogopite, muscovite) are too high compared to those affecting natural resetting of geochronometers due to greater artificially-induced ^{40}Ar loss during heating experiments (Villa, 1994, 2010). During initial heating, insufficient water activity in the experimental capsule leads to dehydroxylation, whereas excessive water activity can result in aqueous dissolution. Both processes may create pathways through which ^{40}Ar can escape more rapidly than in nature, resulting in overestimation of the measured volume diffusivities (Villa, 2010). Corrected activation energies and diffusion coefficients have been estimated for phlogopite (Villa, 2010), however, correction factors are based on an assumed percentage (~6%) of initial fast-pathway ^{40}Ar loss required to fit lines through measured data. As such, the amount of fast-pathway ^{40}Ar loss from biotite during diffusion experiments is not reliably quantifiable, and corrections for fast-pathway ^{40}Ar loss in experimentally determined E_a and D_0 are not built into our models. This may represent a source of uncertainty in the calculated percentages of ^{40}Ar retention, such that biotite may retain more ^{40}Ar in reality than the modeled percentages. Nonetheless, $^{40}Ar/^{39}Ar$ mica dates have, in many settings, been documented to align with those predicted by measured Ar diffusivities and other isotopic systems (i.e., the $^{40}Ar/^{39}Ar$ age of biotite < muscovite < hornblende < U/Pb ages; e.g., Van Schmus et al., 2007; Schneider et al., 2013; Willigers et al., 2001), suggesting that the measured diffusivities are likely close to those operating in nature.

It is important to note that every biotite grain has a P–T region for which it would retain most, if not all of its radiogenic ^{40}Ar, and this P–T region covers broader temperatures at higher pressures. This point remains valid for any set of diffusion parameters (D_0, E_a, V_0), and our numerical uncertainty analysis has shown that Ar retention/release regions in P–T space are robust against changes in diffusion coefficients.

4.2. Interpreting exhumation and cooling

By illustrating how Ar retentivity in biotite varies with pressure, temperature, grain size and residence time, our modeled P–T–% retention plots can be used to help interpret cooling histories from $^{40}Ar/^{39}Ar$ data in a variety of metamorphic terranes. Our modeled ages and core-to-rim age profiles of hypothetical cooling/exhumation scenarios may also inform tectonic interpretations, especially when linked with in-situ $^{40}Ar/^{39}Ar$ data, such as provided by laser ablation.

Mica intra-grain age maps from UV laser spot analyses reveal abundant information, together with step-heating or total-fusion $^{40}Ar/^{39}Ar$ data to provide context. Previous studies have matched measured core-to-rim age profiles with diffusion model results to constrain cooling rates and cooling/exhumation histories (e.g., Kelley and Wartho, 2000; Wartho et al., 2003; Warren et al., 2011, 2012b; Skipton et al., 2017). Interpretations of cooling histories from UV laser age maps may be limited by the spatial resolution (at least 30–50 μm laser spot size usually required) and analytical errors of UV laser spot ages. Intra-grain age complexities and break-off of crystal edges during sample preparation present additional challenges, and the uncertainties inherent in DiffArgP modeling and biotite diffusion parameters (discussed above) necessitate caution when comparing $^{40}Ar/^{39}Ar$ dates with model results. Even so, we consider such comparisons to be the currently best available approach for interpreting $^{40}Ar/^{39}Ar$ dates as related to cooling, crystallisation or excess ^{40}Ar contamination.

4.2.1. High-grade metamorphism

The models suggest that biotite from medium- to high-grade terranes where the thermal peak is ≥600°C would completely lose any pre-peak (inherited) radiogenic Ar, even if peak metamorphism lasted for only 1 Myr (Figs. 1g, 2a, 2d). Possible exceptions include coarse-grained biotite (2–5 mm radii) residing at pressures of ~1 GPa and higher (Fig. 1a, d). Efficient Ar diffusion ≥600°C – even during short-lived thermal maximums – is supported by analyses of Himalayan biotite grains (0.25–0.5 mm radii) metamorphosed at ≥650°C for ~5 Myr, which yielded dates consistent with cooling ages (Mottram et al., 2015). Therefore, our results indicate that biotite that experienced amphibolite- to granulite-facies metamorphism is a candidate for yielding $^{40}Ar/^{39}Ar$ cooling and exhumation ages (clearly an open grain boundary system is also required). In this, our models are in agreement with long-held protocol for interpreting cooling ages from biotite in high-grade metamorphic terranes.

4.2.2. Low-grade and/or short-lived metamorphism

Temperatures attained during peak greenschist or sub-greenschist-facies metamorphism approach, or are lower than, the nominal closure temperature of Ar in biotite ($T_c \approx 300°C$; McDougall and Harrison, 1999). Biotite that crystallised along the prograde path may therefore retain a percentage of pre-thermal peak ^{40}Ar (i.e., its Ar systematics are not fully reset) and produce an $^{40}Ar/^{39}Ar$ date that is older than the cooling age that would be predicted had the biotite crystallised at, and cooled from, peak temperatures. Our models provide graphical representation of this scenario, allowing a quantitative estimate of whether or not inherited Ar could be a factor in biotite of a variety of grain sizes residing at a variety of conditions. For example, a 1 mm-radius biotite grain metamorphosed at 375°C (P >0.5 GPa) would need to remain at those conditions for >20 Myr to retain none of its pre-peak Ar (Figs. 1g–i, 3a–c). If metamorphosed at 375°C for 20 Myr, a coarser-grained crystal (2–5 mm radius) would retain at least ~50% inherited Ar, regardless of pressure (Fig. 1c, f). The models show that biotite grains with smaller radii (~0.1–0.5 mm) are the safest choice for constraining the cooling age following peak greenschist-facies metamorphism. Biotite grains that experienced thermal peak at sub-greenschist-facies (≤300–350°C) are capable of yielding $^{40}Ar/^{39}Ar$ crystallization ages, but not cooling ages. This relationship can potentially be used to date low-temperature events such as fluid-assisted biotite neo- or recrystallization, as has been demonstrated for white mica (e.g., Cossette et al., 2015; Kellett et al., 2016).

Rapid metamorphic cycles, and short residence times at peak conditions, such as appears to be the case in many modern orogens, also present challenges for interpreting $^{40}Ar/^{39}Ar$ ages. Without sufficient time to diffuse out of biotite, pre-peak radiogenic Ar may be retained even in 0.1 mm-radius grains that experienced moderate temperatures. For instance, during 1 Myr residence at medium pressures, our models suggest that a 0.1 mm-radius biotite grain would only be fully reset (retain 0% pre-peak Ar) if temperatures were sustained at ≥400°C (Fig. 2d).

In the eastern Himalaya, biotite ages from an inverted metamorphic sequence (garnet to kyanite-sillimanite grades; 0.4–0.8 GPa) provide empirical evidence of ^{40}Ar inheritance resulting from short-lived metamorphism at moderate temperatures (Mottram et al., 2015). Biotite grains with 0.25 and 0.5 mm radii were dated from the highest-grade part of the sequence, which was metamorphosed at ≥650°C for ~5 Myr, and yielded narrow age populations indicative of cooling ages. In contrast, biotite grains with equivalent radii were analyzed from lower-grade rocks that experienced peak temperatures of 400–580°C for ≤1 Myr. These grains produced discordant heating spectra and dispersed $^{40}Ar/^{39}Ar$ dates that were both older and younger than those of co-existing muscovite (Mottram et al., 2015). The authors attributed this trend to incomplete re-setting of Ar systematics (Ar inheritance) resulting from short residence times at low temperatures. In support of this interpretation, our models illustrate that a 0.5 mm-radius biotite grain experiencing peak temperatures at 400°C and pressures of 0.4–0.8 GPa would need to remain at those conditions for >20 Myr to achieve complete loss of pre-peak ^{40}Ar (Fig. 2b). For a temperature of 580°C, the same grain would lose all pre-peak ^{40}Ar if it remained at those conditions for ≥1 Myr (Fig. 2a).

4.2.3. Precambrian orogens

The models highlight key factors in interpreting $^{40}Ar/^{39}Ar$ ages in Precambrian orogens where rocks are known to have resided at lower-, mid- and/or upper-crustal conditions for 10s to 100s of Myr, or even Gyr timescales. In Precambrian terranes, slow cooling rates of ≤10°C/Myr are typically deduced from comparisons between $^{40}Ar/^{39}Ar$ and U–Pb ages (e.g., Schneider et al., 2007; Rivers, 2008; Willigers et al., 2001; Skipton et al., 2017). Alternatively, it has been proposed that $^{40}Ar/^{39}Ar$ ages in Precambrian terranes may be artificially young due to gradual diffusive Ar loss during long-term crustal residence below nominal Ar closure temperatures (Dunlap, 2000). As a result, rates of cooling and exhumation in Precambrian terranes may have been faster than current estimations. Our modeled P–T–%retention plots support limited Ar loss during long-term, low-temperature crustal residence of fine-grained biotite. For instance, a 0.1 mm-radius biotite grain may lose ~25% of its Ar during 1 Gyr of residence at 200°C and 0.3 GPa, and ~70% at 275°C (Fig. 3i). However, models of 0.5 mm-radius biotite that resided at 250°C for 500 Myr and 1 Gyr exhibit flat core-to-rim age profiles with Ar loss evident only in the outermost ~50 μm of grain edges (Figs. 5b, 6a). The bulk ages of these models are up to 84 Myr younger than the onset of crustal residence at 250°C. Our modeling therefore implies that long-term crustal residence at $T < T_c$ may produce a bulk $^{40}Ar/^{39}Ar$ date several Myr younger than the age of cooling through T_c, and that diffusive Ar loss may be detectable within the grain edge using UV laser $^{40}Ar/^{39}Ar$ spot core-to-rim transects.

UV age transects have been compared with DiffArgP models to test cooling rates and low-temperature Ar loss in muscovite from the Paleoproterozoic Trans-Hudson Orogen (Skipton et al., 2017). In that case, core-to-rim age profiles generated by DiffArgP models of 1 Gyr isothermal residence at 220°C exhibited minor Ar loss at muscovite grain edges, which coincided with dates of UV laser spots. Due to the 50 μm UV spot size and analytical (and model) uncertainties, this relationship was not definitive, but supports the plausibility of gradual Ar loss during long-term isothermal residence at $T < T_c$. Importantly, in that study, DiffArgP models simulating various initial cooling rates (1–10°C/Myr) showed that any slow Ar loss that may have occurred during a subsequent 1 Gyr isothermal period in the crust (at T = 220°C) would have been insufficient to change cooling ages beyond uncertainties, or to erase Ar evidence of early rapid (≥10°C/Myr) cooling. Therefore, the muscovite likely cooled at 1–2.5°C/Myr following peak metamorphism, in line with 'slow' cooling rates determined in other Precambrian orogens (Skipton et al., 2017).

UV laser spot intra-grain $^{40}Ar/^{39}Ar$ age maps also revealed evidence of slow cooling in biotite from a ca. 1680 Ma synorogenic monzogranite in the Yavapai orogen in the southwestern United States (Hodges and Bowring, 1995). The authors concluded that core-to-rim age decreases of ~200 Myr (from ca. 1240 to 1040 Ma) over 0.5–0.7 mm grain radiii resulted from slow cooling following magmatic crystallization, in agreement with independent geological evidence. They used the closure temperature algorithm (Dodson, 1986) to estimate a cooling rate of 0.5 K/Myr. This estimate is supported by our DiffArgP models: models using a faster cooling rate of 1.5°C/Myr yielded more shallowly sloped core-to-rim age gradients (~100 Myr; Figs. 4e–f, 5e–f, 6c) than that of the Yavapai biotite.

In some Proterozoic orogens, faster cooling rates have been interpreted from $^{40}Ar/^{39}Ar$ ages that are nearly equivalent to metamorphic U/Pb ages. Mid-crustal blocks in the Grenville orogen appear to have cooled at rates up to 11°C/Myr during late-orogenic extension (Cosca et al., 1995; Rivers, 2008; Schneider et al., 2013). Gravity-driven extensional collapse has been proposed in the Variscan orogen, based on rapid cooling and exhumation deduced in part from

$^{40}Ar/^{39}Ar$ ages (e.g., Steltenpohl et al., 1993). “Old” biotite dates that are similar to U/Pb ages of peak metamorphism, suggesting fast cooling, may be reliable if Ar inheritance is ruled out. This can be evaluated using our model results, together with the known P–T history: the dated biotite must have resided for sufficient time at temperatures in the ‘blue’ P–T zones (in Figs. 1–3). Theoretically, it would also exhibit a flat core-to-rim age profile indicating rapid cooling (e.g., age profiles for cooling rates of 10°C/Myr and 30°C/Myr in Figs. 4e–f, 5e–f, 6c). However, such an interpretation assumes no excess Ar contamination, a completely open grain boundary and no trapping of Ar within grain defects; these assumptions are challenging to quantify (discussed below).

4.3. Effects of extraneous Ar and fast-pathway Ar loss

By showing the ages that would be expected following volume diffusion acting alone, our models can help determine whether a biotite $^{40}Ar/^{39}Ar$ date is likely to represent the timing of cooling at a particular rate or if it could have been produced or reset by other processes.

The effects on $^{40}Ar/^{39}Ar$ cooling ages of crystal defects serving as Ar traps (e.g., Camacho et al. 2012) or Ar-loss pathways (e.g., Lee, 1995; Hodges and Bowring, 1995) cannot be directly tested using DiffArgP models. Instead, P–T–%retention plots (Figs. 1–3) provide theoretical constraints on alternative scenarios: e.g., an anomalously young biotite age may result from late, low-temperature biotite crystallization within the ‘red zones’, and not necessarily from Ar loss through grain defects. UV laser spot analyses are important for investigating possible effects of crystal defects on Ar ages; anomalously young zones within biotite may be attributed to grain defects allowing rapid Ar loss (e.g., Hodges and Bowring, 1995; Skipton et al., 2017).

The P–T–% retention plots (Figs. 1–3) can be used to assess the likelihood of retention of inherited Ar: biotite that experienced peak conditions within the red or intermediate P–T zones is at risk for containing pre-thermal peak radiogenic Ar, producing an $^{40}Ar/^{39}Ar$ age that may predate the timing of post-thermal peak cooling through T_c. Conversely, if biotite experienced peak P–T in the blue zone, yet yields an $^{40}Ar/^{39}Ar$ age that is older than that expected from independent data, the biotite may have been contaminated by excess ^{40}Ar ($^{40}Ar_e$).

In some cases, $^{40}Ar_e$ contamination can be identified from step-heating analyses (review in Kelley, 2002). $^{40}Ar_e$ has been suggested as the cause of saddle-shaped gas release spectra (Lanphere and Dalrymple, 1976; Harrison and McDougall, 1981; McDougall and Harrison, 1999); the shape arising from the suggested release of ^{40}Ar trapped in fluid or melt inclusions at low temperature and from the breakdown of solid inclusions at high temperature (Kelley, 2002).

A linear array of step-heating data on an inverse isochron plot may also show the presence of trapped $^{40}Ar_e$ with a distinct non-atmospheric composition (Heizler and Harrison, 1988). However, identification of an $^{40}Ar_e$ component on an isochron plot may be prevented by scattered data, which results from $^{40}Ar_e$ with an inhomogeneous isotopic ratio (e.g., inclusions; Reddy et al., 1997) or, possibly, clustered data resulting from homogenization with radiogenic Ar produced in situ (at $T > T_c$). Additionally, anomalously old biotite ages are commonly calculated from flat ‘plateau’ gas release spectra (e.g., Pankhurst et al., 1973; Roddick et al., 1980; Sherlock et al., 1999; Skipton et al., 2017). In such cases, there is currently no definitive test for $^{40}Ar_e$ contamination, and DiffArgP modeling does not provide one.

DiffArgP can, however, be used to model diffusion of excess Ar from the grain boundary network into the grain, and comparisons with intra-grain UV laser age spots can shed light on how/when excess Ar may have been incorporated. For example, in white mica from the Oman high-pressure terrane, UV laser spot transects revealed Ar enrichment in grain rims (Warren et al., 2011). The authors ran DiffArgP models in which excess Ar was introduced to the grain boundary network (the 'edge age' in Wheeler, 1996) at different times along the cooling path. When excess Ar was introduced in the models at 'low' temperatures (i.e., temperatures approaching T_c), the modeled core-to-rim age profiles exhibited Ar-enriched grain rims with anomalously old bulk ages. This led the authors to conclude that the anomalously old white mica could have incorporated excess Ar late in the cooling history from grain boundary fluids in a closed system, through diffusion or incorporation during recrystallization (Warren et al., 2011). In a similar case, $^{40}Ar/^{39}Ar$ UV laser transects conducted across biotite grains from the Italian Alps yielded dates that increased from core to rim, ranging from ca. 161 to 514 Ma in individual crystals (Pickles et al., 1997). This age pattern was attributed to diffusion of excess Ar into the grains at temperatures less than 300°C, as supported by theoretically derived curves for volume diffusion of Ar (Pickles et al., 1997).

Incorporation of $^{40}Ar_e$ at high temperatures (>T_c, in blue zones in Figs. 1–3), at which Ar diffusion is highly efficient, would theoretically result in diffusive within-grain homogenization of the excess Ar with radiogenic ^{40}Ar produced *in situ*. As such, the mica would yield an anomalously old age and a smoothly decreasing core-to-rim age profile; this has been illustrated by DiffArgP models of white mica (Warren et al., 2011). Therefore, biotite that yields an anomalously old age but a smoothly decreasing core-to-rim age profile with no evidence of ^{40}Ar-enrichment at grain rims may still contain excess Ar. In this case, biotite would have had to have incorporated $^{40}Ar_e$ during (or prior to) peak P–T conditions in the blue zones in Figs. 1–3, either via diffusion from ^{40}Ar-enriched metamorphic fluids, or incorporation during crystallisation in the presence of ^{40}Ar-enriched fluids. In contrast, excess Ar enrichment of rims is likely to have occurred at maximum P–T conditions in the red or intermediate zones, such as via low-temperature diffusion from a ^{40}Ar-enriched grain boundary network in a closed system. Our P–T–% retention plots can thus be used in conjunction with the established P–T history to evaluate scenarios of $^{40}Ar_e$ contamination.

Figs. 1i, 2c and 2f compare modeled Ar retentivity in biotite (this study) and muscovite (Warren et al., 2012a) for grain radii of 0.1, 0.5 and 1 mm with 20 Myr residence. The model data reiterate previously established points: muscovite requires higher temperatures than biotite to achieve diffusional loss of pre-thermal peak Ar and resetting of ^{40}Ar/^{39}Ar systematics, and has a higher nominal closure temperature. Therefore, the ^{40}Ar/^{39}Ar cooling age of biotite should be younger than that of muscovite in the same rock, provided both minerals grew during the same metamorphic event within the 'blue' P–T zones modeled for biotite (Figs. 1–3) and muscovite (Figs. 3 and 4 in Warren et al., 2012a). Nonetheless, as discussed above, some paired biotite and muscovite ages defy this theoretical relationship. In such cases, muscovite may have crystallized or recrystallized at low temperatures, following cooling through the biotite nominal closure temperature, i.e., within the 'red' P–T zones. A known P–T history is crucial for interpreting this scenario, together with petrographical evidence of late white mica growth/recrystallization. Mica chemistry can also be used to elucidate recrystallized, compositionally distinct muscovite rims (e.g., Cossette et al., 2015). Still, muscovite with no apparent evidence of low-temperature ($<T_c$) growth, compositional zoning or recrystallization has been shown to yield ages younger than those of co-existing biotite in some cases (e.g., Mottram et al., 2015; Skipton et al., 2017). Due to the higher solubility of Ar in biotite than muscovite, biotite may preferentially incorporate $^{40}Ar_e$ (Roddick et al., 1980; Dahl, 1996; review in Kelley, 2002). Anomalously old biotite ages

may result from planar defects in the crystal acting as Ar traps (Camacho et al., 2012). In cases where biotite yields an older $^{40}Ar/^{39}Ar$ age than co-existing muscovite, obtaining UV laser spot transects on both minerals would inform considerations of $^{40}Ar_e$, particularly if localized ^{40}Ar-enriched zones were revealed. Notably, there are currently few intra-grain age data for biotite (Hodges and Bowring, 1995; Pickles et al., 1997) or for co-existing muscovite, which might otherwise be used to further constrain this discussion.

5. Conclusions

The models presented here provide numerical and visual illustration of the percentage of Ar that should theoretically be retained in biotite with a variety of grain radii (0.1 to 5 mm) residing for various periods (1 Myr to 1 Gyr) over a range of P–T conditions (Figs. 1–3). The models also demonstrate the effects of different crustal residence temperatures (250–450°C) and durations (1 Myr to 1 Gyr), and of various subsequent cooling rates (1.5–30°C/Myr), on the $^{40}Ar/^{39}Ar$ age and core-to-rim age profile of biotite (Figs. 4–6). Consequently, the models are effective for interpreting metamorphic $^{40}Ar/^{39}Ar$ ages and corresponding cooling/exhumation histories in modern and ancient orogens. As they represent a baseline for %Ar retention, $^{40}Ar/^{39}Ar$ ages and intra-grain age profiles of biotite that are expected from volume diffusion acting alone, the models are useful for evaluating the likelihood of extraneous ^{40}Ar contamination and non-diffusional ^{40}Ar loss.

The models presented here demonstrate the importance of interpreting $^{40}Ar/^{39}Ar$ ages within an established P–T–t framework: the dated crystal must have attained peak P–T conditions within the ‘blue’ zones (Figs. 1–3) in order to yield a cooling age. Petrographic analyses, mineral chemical maps and an understanding of the P–T evolution are also key to assessing whether mica recrystallization or dissolution may have reset Ar systematics. An ^{40}Ar/^{39}Ar biotite age should be supplemented by a muscovite age from the same rock when possible, which provides an additional constraint on the cooling/exhumation history, especially in conjunction with P–T–%retention plots for biotite (this study) and muscovite (Warren et al., 2012a). Paired biotite–muscovite ages may also provide insights into excess ^{40}Ar contamination.

The modeled core-to-rim age profiles for biotite presented here strongly support the UV laser spot technique for ^{40}Ar/^{39}Ar thermochronological studies. Intra-grain age maps have the potential to yield a wealth of information, including diffusional core-to-rim age profiles from which cooling histories can be interpreted, particularly when compared with diffusion models, as demonstrated in previous studies. UV laser age maps also enable assessment of: excess ^{40}Ar; inherited ^{40}Ar; ^{40}Ar loss via fast-diffusion pathways (anomalously young ages in grain centre); and, possibly, low-temperature ($<T_c$) diffusional Ar loss from grain rims during long-term crustal residence.

Cooling/exhumation histories, as classically interpreted from ^{40}Ar/^{39}Ar data, must be grounded in theoretical diffusional behaviour, as quantified by DiffArgP modeled bulk ages and core-to-rim age profiles. The temperature, pressure, time and grain-size parameters used in our models correspond to many geological scenarios, and the models can therefore be compared with ^{40}Ar/^{39}Ar biotite ages to inform interpretations of cooling/exhumation. For geological parameters beyond those modeled here, we recommend using DiffArgP to model proposed cooling histories for comparisons with ^{40}Ar/^{39}Ar results.

The models presented here contain several sources of uncertainty. They are therefore best used in conjunction with ^{40}Ar/^{39}Ar biotite data to provide approximate P–T–t constraints on interpreted cooling/exhumation histories or to highlight alternative scenarios, rather than to provide a single ‘answer’. Further research to improve constraints on Ar behaviour in biotite will increase confidence in biotite $^{40}Ar/^{39}Ar$ ages as relating to geological phenomena linked to time, rather than contamination. In particular, new UV laser $^{40}Ar/^{39}Ar$ spot maps of biotite from various metamorphic terranes would provide a more complete library of intra-grain Ar distributions in biotite for comparison with diffusion models, and are an important step toward developing methodology for identifying and quantifying excess Ar and Ar trapped or lost via grain defects in biotite.

Acknowledgements

DRS acknowledges support from the Alice Wilson Postdoctoral Fellowship, Geological Survey of Canada. Dawn Kellett and David Schneider are thanked for fruitful discussions on $^{40}Ar/^{39}Ar$ thermochronology in biotite. Geological Survey of Canada Lands and Minerals Sector Contribution Number #####.

References

Berger, G.W., 1975. $^{40}Ar/^{39}Ar$ step heating of thermally over-printed biotites, hornblendes, and potassium feldspars from Eldora, Colorado. Earth and Planetary Science Letters 26, 387–408.

Brewer, M.S., 1969. Excess radiogenic argon in metamorphic micas from the Eastern Alps, Austria. Earth and Planetary Science Letters 6, 321–331.

Camacho, A., Lee, J.K.W., Fitz Gerald, J.D., Zhao, J., Abdu, Y.A., Jenkins, D.M., Hawthorne, F.C., Kyser, T.K., Creaser, R.A., Armstrong, R., Heaman, L.W., 2012. Planar defects as

Ar traps in trioctahedral micas: A mechanism for increased Ar retentivity in phlogopite. Earth and Planetary Science Letters 341–344, 255–267.

Cosca, M.A., Sutter, J.F., Essene, E.J., 1991. Cooling and inferred uplift/erosion history of the Grenville Orogen, Ontario: constraints from $^{40}Ar/^{39}Ar$ thermochronology. Tectonics 10 (5), 959–977.

Cosca, M.A., Essene, E.J., Mezger, K., van der Pluijm, B.A., 1995. Constraints on the duration of tectonic processes: Protracted extension and deep-crustal rotation in the Grenville orogen. Geology 23 (4), 361–364.

Cossette, E., Schneider, D.A., Warren, C.J., Grasemann, B., 2015. Lithological, rheological, and fluid infiltration control on $^{40}Ar/^{39}Ar$ ages in polydeformed rocks from the West Cycladic detachment system, Greece. Lithosphere 7 (2), 189–205.

Dahl, P.S., 1996. The crystal-chemical basis for Ar retention in micas: inferences from interlayer partitioning and implications for geochronology. Contributions to Mineralogy and Petrology 123, 22–39.

Dallmeyer, R.D., Rivers, T., 1983. Recognition of extraneous argon components through incremental-release $^{40}Ar/^{39}Ar$ analysis of biotite and hornblende across the Grenvillian metamorphic gradient in southwestern Labrador. Geochimica et Cosmochimica Acta 47, 413–428.

Dodson, M.H., 1973. Closure temperature in cooling geochronological and petrological systems. Contributions to Mineralogy and Petrology 40, 259–274.

Dodson, M.H., 1986. Closure profiles in cooling systems. Materials Science Forum 7, 145–154.

Dunlap, W.J., 2000. Nature's diffusion experiment: The cooling-rate cooling-age correlation. Geology 28 (2), 139–142.

Foland, K.A., 1983. $^{40}Ar/^{39}Ar$ incremental heating plateaus for biotites with excess argon. Isotope Geoscience 1(1), 3–21.

Forster, M.A., Lister, G.S., 2014. $^{40}Ar/^{39}Ar$ geochronology and the diffusion of ^{39}Ar in phengite-muscovite intergrowths during step-heating experiments in vacuo. In: Jourdan, F., Mark, D.F., Verati, C. (eds) 2014. Advances in $^{40}Ar/^{39}Ar$ Dating: from Archeology to Planetary Sciences. Geological Society, London, Special Publications 378, 117–135.

Gaber, L.J., Foland, K.A., Corbató, C.E., 1988. On the significance of argon release from biotite and amphibole during $^{40}Ar/^{39}Ar$ vacuum heating. Geochimica et Cosmochimica Acta 52, 2457–2465.

Giletti, B.J., 1974. Studies in diffusion I. Argon in phlogopite mica. In: Geochemical Transport and Kinetics, Carnegie Institute of Washington Publication, 107–115.

Giletti, B.J., Tullis, J., 1977. Studies in diffusion IV: Pressure dependence of Ar diffusion in phlogopite mica. Earth and Planetary Science Letters 35, 180–183.

Grove, M., 1993. Thermal histories of Southern California basement terranes. Ph.D. Thesis. University of California, Los Angeles, 419 pp.

Grove, M., Harrison, T.M., 1996. $^{40}Ar^{*}$ diffusion in Fe-rich biotite. American Mineralogist 81, 940–951.

Hames, W.E., Bowring, S.A., 1994. An empirical evaluation of the argon diffusion geometry in muscovite. Earth and Planetary Science Letters 124 (1–4), 161–169.

Hanson, G.N., Simmons, K.R., Bence, A.E., 1975. ^{40}Ar/^{39}Ar spectrum ages for biotite, hornblende and muscovite in a contact metamorphic zone. Geochimica et Cosmochimica Acta 39, 1269–1277.

Harrison, T.M., Duncan, I., McDougall, I., 1985. Diffusion of ^{40}Ar in biotite: Temperature, pressure and compositional effects. Geochimica et Cosmochimica Acta 49, 2461–2468.

Harrison, T.M., Célérier, J., Aikman, A.B., Hermann, J., Heizler, M.T., 2009. Diffusion of ^{40}Ar in muscovite. Geochimica et Cosmochimica Acta 73, 1039–1051.

Harrison, T.M., McDougall, I., 1981. Excess ^{40}Ar in metamorphic rocks from Broken Hill, New South Wales: implications for ^{40}Ar/^{39}Ar age spectra and the thermal history of the region. Earth and Planetary Science Letters 55, 123–149.

Heizler, M.T., Harrison, T.M., 1988. Multiple trapped argon isotope components revealed by ^{40}Ar/^{39}Ar isochron analysis. Geochimica Cosmochimica Acta 52, 1295–1303.

Hodges, K.V., Bowring, S.A., 1995. ^{40}Ar/^{39}Ar thermochronology of isotopically zoned micas: Insights from the southwestern USA Proterozoic orogeny. Geochimica et Cosmochimica Acta 59 (15), 3205–3220.

Kellett, D.A., Warren, C.J., Larson, K.P., Zwingmann, H., van Staal, C.R., Rogers, N., 2016. Influence of deformation and fluids on Ar retention in which mica: Dating the Dover Fault, Newfoundland Appalachians. Lithos 254–255, 1–17.

Kelley, S., 2002. Excess argon in K–Ar and Ar–Ar geochronology. Chemical Geology 188, 1–22.

Kelley, S.P., Wartho, J.-A., 2000. Rapid kimberlite ascent and the significance of Ar-Ar ages in xenolith phlogopites. Science 289, 609–611.

Lanphere, M.A., Dalrymple, G.B., 1976. Identification of excess ^{40}Ar by the $^{40}Ar/^{39}Ar$ age spectrum technique. Earth and Planetary Science Letters 32, 141–148.

Lee, J.K.W., 1995. Multipath diffusion in geochronology. Contributions to Mineralogy and Petrology 120, 60–82.

Lee, J.-Y., Marti, K., Severinghaus, J.P., Kawamura, K., Yoo, H.-S., Lee, J.B., Kim, J.S., 2006. A redetermination of the isotopic abundances of atmospheric Ar. Geochimica et Cosmochimica Acta 70, 4507–4512.

McDougall, I., Harrison, T.M., 1999. Geochronology and Thermochronology by the $^{40}Ar/^{39}Ar$ Method. Oxford University Press, New York, New York, 269 pp. (2nd Ed.).

Mottram, C.M., Warren, C.J., Halton, A.M., Kelley, S.P., Harris, N.B.W., 2003. Argon behaviour in an inverted Barrovian sequence, Sikkim Himalaya: The consequences of temperature and timescale on $^{40}Ar/^{39}Ar$ mica geochronology. Lithos 238, 37–51.

Occhipinti, S.A., Reddy, S.M., 2009. Neoproterozoic reworking of the Palaeoproterozoic Capricorn Orogen of Western Australia and implications for the amalgamation of Rodinia. In: Murphy, J.B., Keppie, J.D., Hynes, A.J. (Eds.) Ancient Orogens and Modern Analogues. Geological Society, London, Special Publications 327, 445–456.

Pankhurst, R.J., Moorbath, S., Rex, D.C., Turner, G., 1973. Mineral age patterns in ca. 3700 my old rocks from West Greenland. Earth and Planetary Science Letters 20, 157–170.

Pickles, C.S., Kelley, S.P., Reddy, S.M., Wheeler, J., 1997. Determination of high spatial resolution argon isotope variations in metamorphic biotites. Geochimica et Cosmochimica Acta 61 (18), 3809–3833.

Reddy, S.M., Kelley, S.P., Magennis, L., 1997. A microstructural and argon laserprobe study of shear zone development at the western margin of the Nanga Parbat – Haramosh Massif, western Himalaya. Contributions to Mineralogy and Petrology 128, 16–29.

Rivers, T., 2008. Assembly and preservation of lower, mid, and upper orogenic crust in the Grenville Province – Implications for the evolution of large hot long-duration orogens. Precambrian Research 167, 237–259.

Roddick, J.C., Cliff, R.A., Rex, D.C., 1980. The evolution of excess argon in alpine biotites – a ^{40}Ar–^{39}Ar analysis. Earth and Planetary Science Letters 48, 185–208.

Schneider, D.A., Edwards, M.A., Kidd, W.S.F., Asif Khan, M., Seeber, L., Zeitler, P.K., 1999. Tectonics of Nanga Parbat, western Himalaya: Synkinematic plutonism within doubly vergent shear zones of a crustal-scale pop-up structure. Geology 27 (11), 999–1002.

Schneider , D.A., Heizler, M.T., Bickford, M.E., Wortman, G.L., Condie, K.C., Perilli, S., 2007. Timing constraints of orogeny to cratonization: Thermochronology of the Paleoproterozoic Trans-Hudson orogen, Manitoba and Saskatchewan, Canada. Precambrian Research 153, 65–95.

Schneider, D.A., Cope, N., Holm, D.K., 2013. Thermochronology of the Mont Laurier terrane, southern Canadian Grenville Province, and its bearing on defining orogenic architecture. Precambrian Research 226, 43–58.

Sherlock, S.C., Arnaud, N.O., 1999. Flat plateau and impossible isochrons: apparent 40Ar-39Ar geochronology in a high-pressure terrain. Geochimica et Cosmochimica Acta 63(18), 2835–2838.

Skipton, D.R., Schneider, D.A., McFarlane, C.R.M., St-Onge, M.R., Jackson, S.E., 2016. Multi-stage zircon and monazite growth revealed by depth profiling and in situ U-Pb geochronology: Resolving the Paleoproterozoic tectonics of the Trans-Hudson Orogen on southeastern Baffin Island, Canada. Precambrian Research 285, 272–298.

Skipton, D.R., Schneider, D.A., Kellett, D.A., Joyce, N.L., 2017. Deciphering the Paleoproterozoic cooling history of the northeastern Trans-Hudson Orogen, Baffin Island (Canada), using $^{40}Ar/^{39}Ar$ step-heating and UV laser thermochronology. Lithos 284–285, 69–90.

Smith, P.E., York, D., Easton, R.M., Özdemir, Ö., Layer, P.W., 1994. A laser $^{40}Ar/^{39}Ar$ study of minerals across the Grenville Front: investigations of reproducible excess Ar patterns. Canadian Journal of Earth Sciences 31 (5), 808–817.

Steltenpohl, M.G., Cymerman, Z., Krogh, E.J., Kunk, M.J., 1993. Exhumation of eclogitized continental basement during Variscan lithospheric delamination and gravitational collapse, Sudety Mountains, Poland. Geology 21, 1111–1114.

Stübner, K., Warren, C.J., Ratschbacher, L., Sperner, B., Kleeberg, R., Pfänder, J., Grujic, D., 2017. Anomalously old biotite $^{40}Ar/^{39}Ar$ ages in the NW Himalaya. Lithosphere 9 (3), 366–383.

Warren, C.J., Sherlock, S.C., Kelley, S.P., 2011. Interpreting high-pressure phengite $^{40}Ar/^{39}Ar$ laserprobe ages: an example from Saih Hatat, NE Oman. Contributions to Mineralogy and Petrology 161, 991–1009.

Warren, C.J., Hanke, F., Kelley, S.P., 2012a. When can muscovite $^{40}Ar/^{39}Ar$ dating constrain the timing of metamorphic exhumation? Chemical Geology 291, 79–86.

Warren, C.J., Kelley, S.P., Sherlock, S.C., McDonald, C.S., 2012b. Metamorphic rocks seek meaningful cooling rate: Interpreting $^{40}Ar/^{39}Ar$ ages in an exhumed ultra-high pressure terrane. Lithos 155, 30–48.

Wartho, J.-A., Kelley, S.P., 2003. $^{40}Ar/^{39}Ar$ ages in mantle xenolith phlogopites: determining the ages of multiple lithospheric mantle events and diatreme ascent rates in southern Africa and Malaita, Solomon Islands. Vance, D., Müller, W., Villa, I.M. (eds) Geochronology: Linking the Isotopic Record with Petrology and Textures. Geological Society, London, Special Publications 220, 231–248.

Willigers, B.J.A., Krogstad, E.J., Wijbrans, J.R., 2001. Comparison of thermochronometers in a slowly cooled granulite terrain: Nagssugtoqidian Orogen, West Greenland. Journal of Petrology 42 (9), 1729–1749.

Wheeler, J., 1996. DiffArg: A program for simulating argon diffusion profiles in minerals. Computers and Geosciences 22(8), 919–929.

Van Schmus, W.R., Schneider, D.A., Holm, D.K., Dodson, S., Nelson, B.K., 2007. New insights into the southern margin of the Archean–Proterozoic boundary in the north-central United States based on U–Pb, Sm–Nd, and Ar–Ar geochronology. Precambrian Research 157, 80–105.

Viete, D.R., Forster, M.A., Lister, G.S., 2011. The nature and origin of the Barrovian metamorphism, Scotland: $^{40}Ar/^{39}Ar$ apparent age patterns and the duration of metamorphism in the biotite zone. Journal of the Geological Society, London 168, 133–146.

Villa, I.M., 1994. Multipath Ar transport in K-feldspar deduced from isothermal heating experiments. Earth and Planetary Science Letters 122, 393–401.

Villa, I.M., 2010. Disequilibrium textures versus equilibrium modeling: geochronology at the crossroads. In: Spalla, M.I., Marotta, A.M. and Gosso, G. (eds) Advances in Interpretation of Geological Processes: Refinement of Multi-scale Data and Integration in Numerical Modelling. Geological Society, London, Special Publications 332, 1–15.

Zimmerman, J.-C., 1972. Water and gas in the main silicate families: Distribution and application to geochronology and petrogenesis. Sciences Terre Memoir 2, 188 pp.

Figures

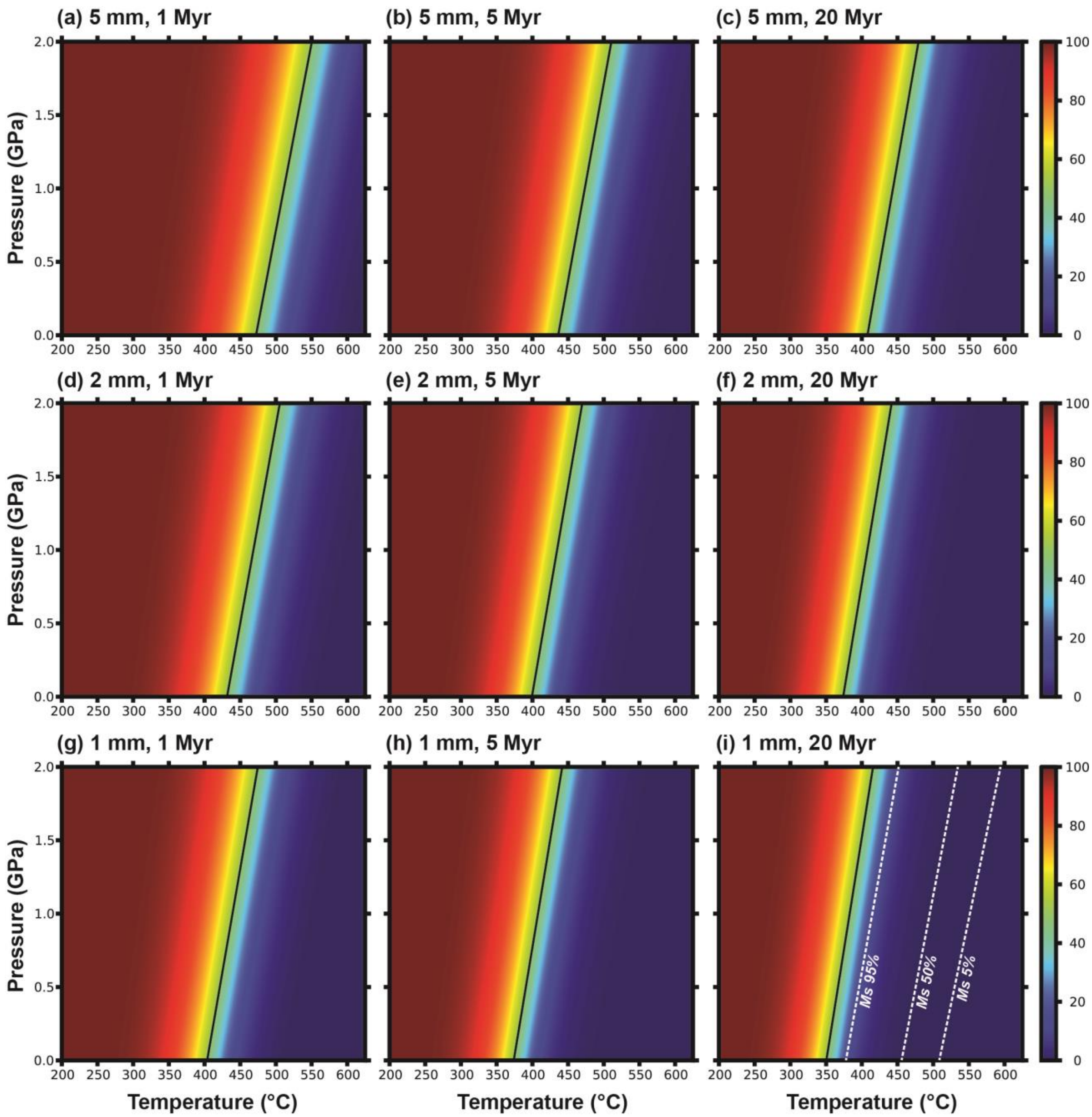

Fig. 1: Pressure–temperature diagrams colour coded with percentages of radiogenic Ar retained in biotite, as calculated from numerical diffusion models for biotite grains with radii of 1, 2 and 5 mm residing at the given P–T conditions for periods of 1, 5 and 20 Myr. White dashed lines indicate percentages of radiogenic Ar retained in muscovite, modelled by Warren et al. (2012).

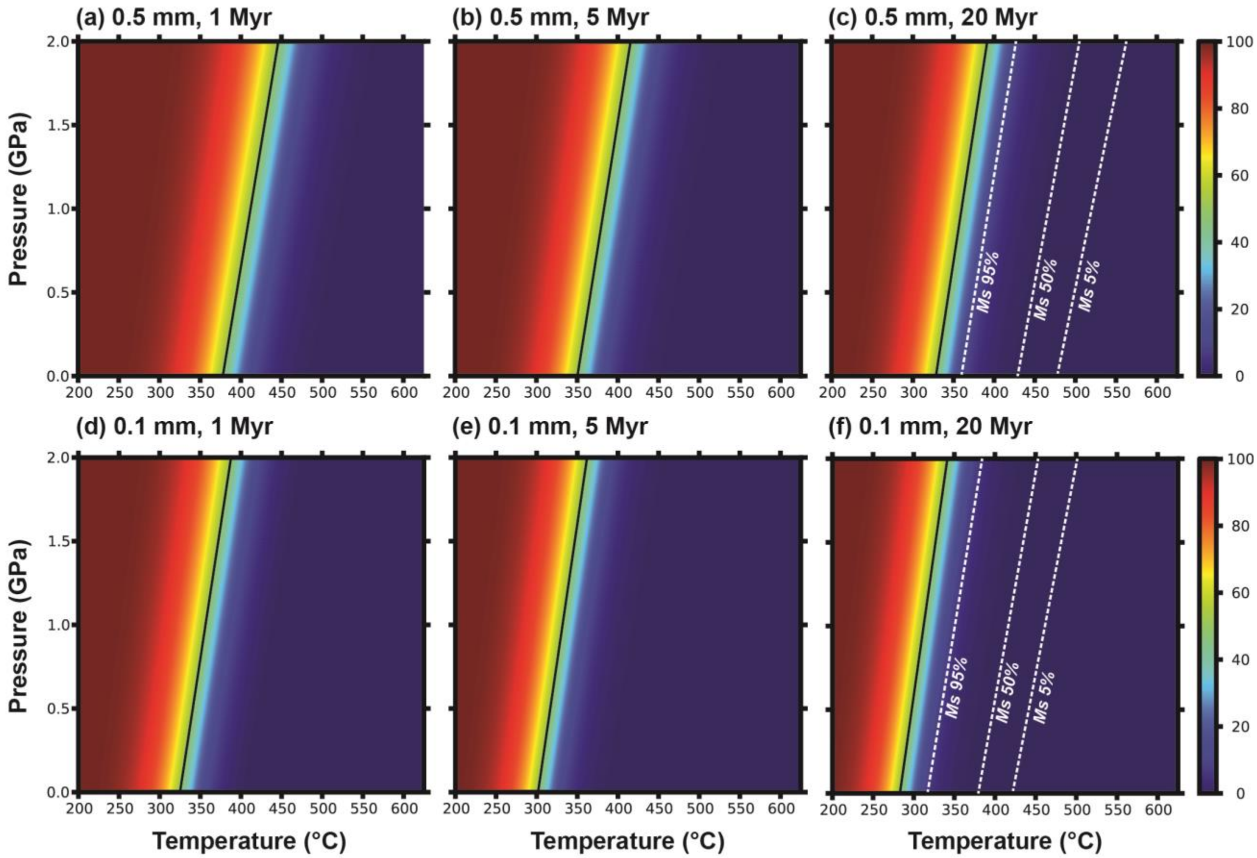

Fig. 2: Pressure–temperature diagrams colour coded with percentages of radiogenic Ar retained in biotite, as calculated from numerical diffusion models for biotite grains with radii of 0.5 and 0.1 mm residing at the given P–T conditions for periods of 1, 5 and 20 Myr. White dashed lines indicate percentages of radiogenic Ar retained in muscovite, modelled by Warren et al. (2012).

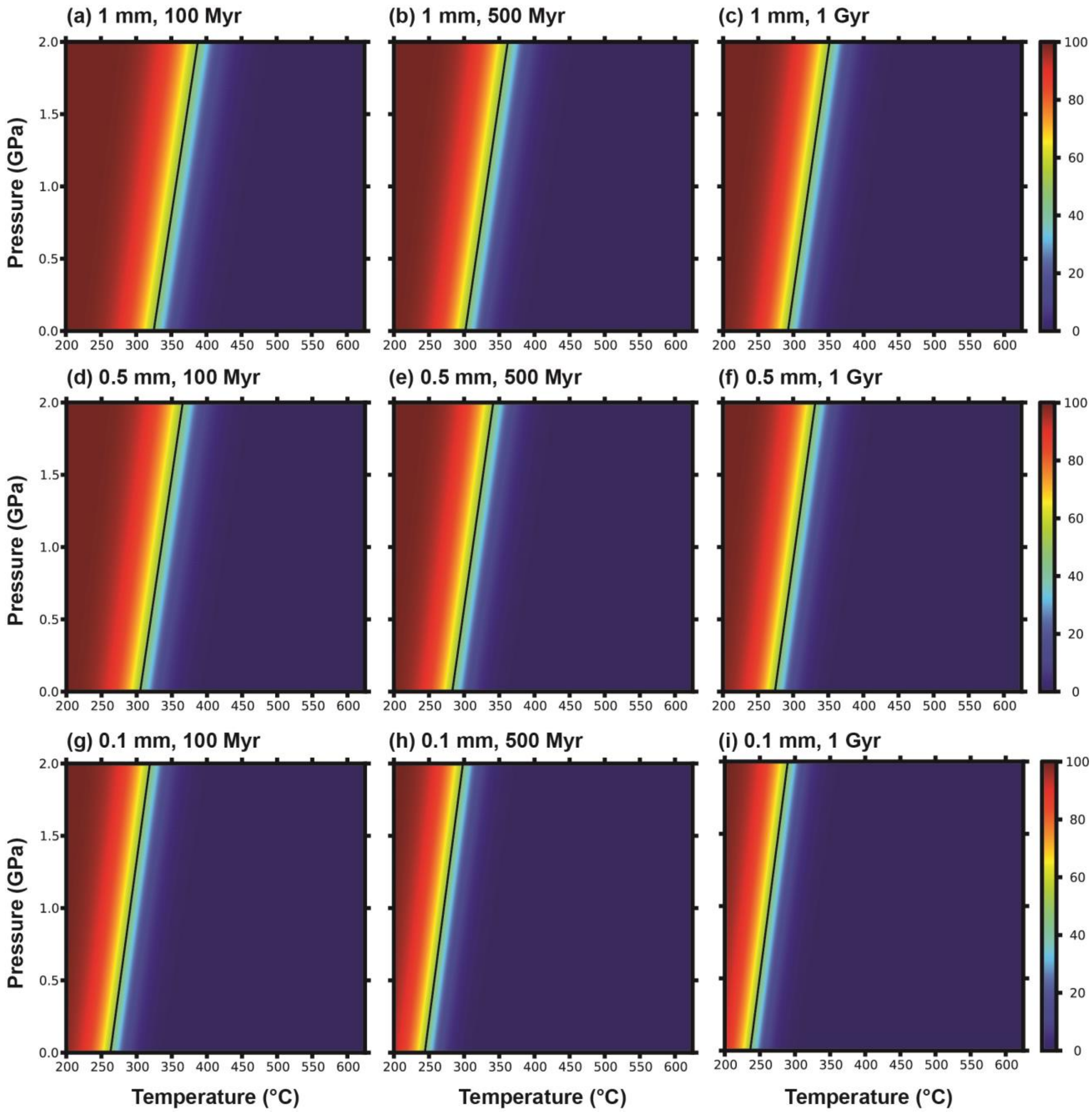

Fig. 3: Pressure–temperature diagrams colour coded with percentages of radiogenic Ar retained in biotite, as calculated from numerical diffusion models for biotite grains with radii of 1, 0.5 and 0.1 mm residing at the given P–T conditions for periods of 100 Myr, 500 Myr and 1 Gyr.

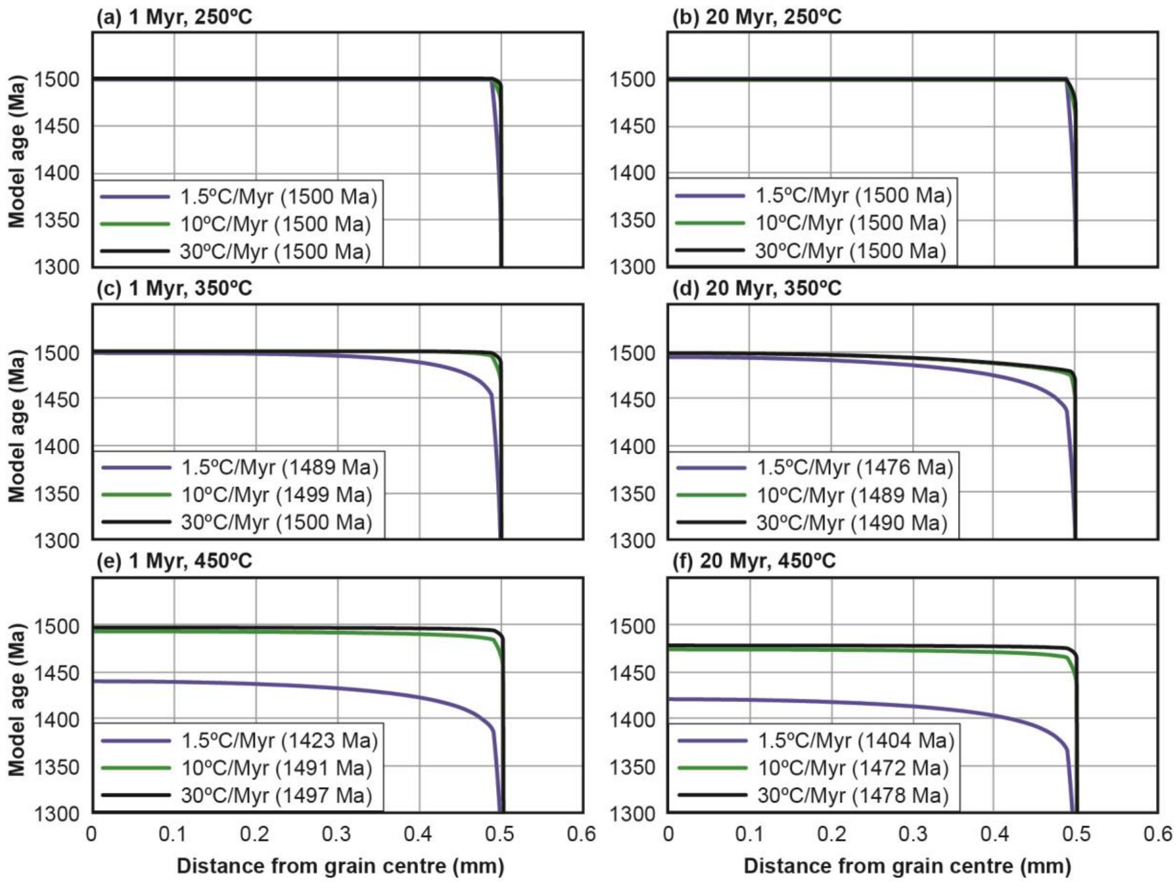

Fig. 4: Modelled core-to-rim $^{40}Ar/^{39}Ar$ age profiles for 0.5 mm-radius biotite that remained at temperatures of 250°C, 350°C or 450°C for 1 Myr or 20 Myr, then cooled at rates of 1.5°C/Myr, 10°C/Myr or 30°C/Myr. All models were run with an initial pressure of 0.7 GPa, followed by decompression that occurred simultaneously with cooling. Models were run from an arbitrary starting time of 1500 Ma; see text for details. Model bulk ages are shown in parentheses for each cooling rate.

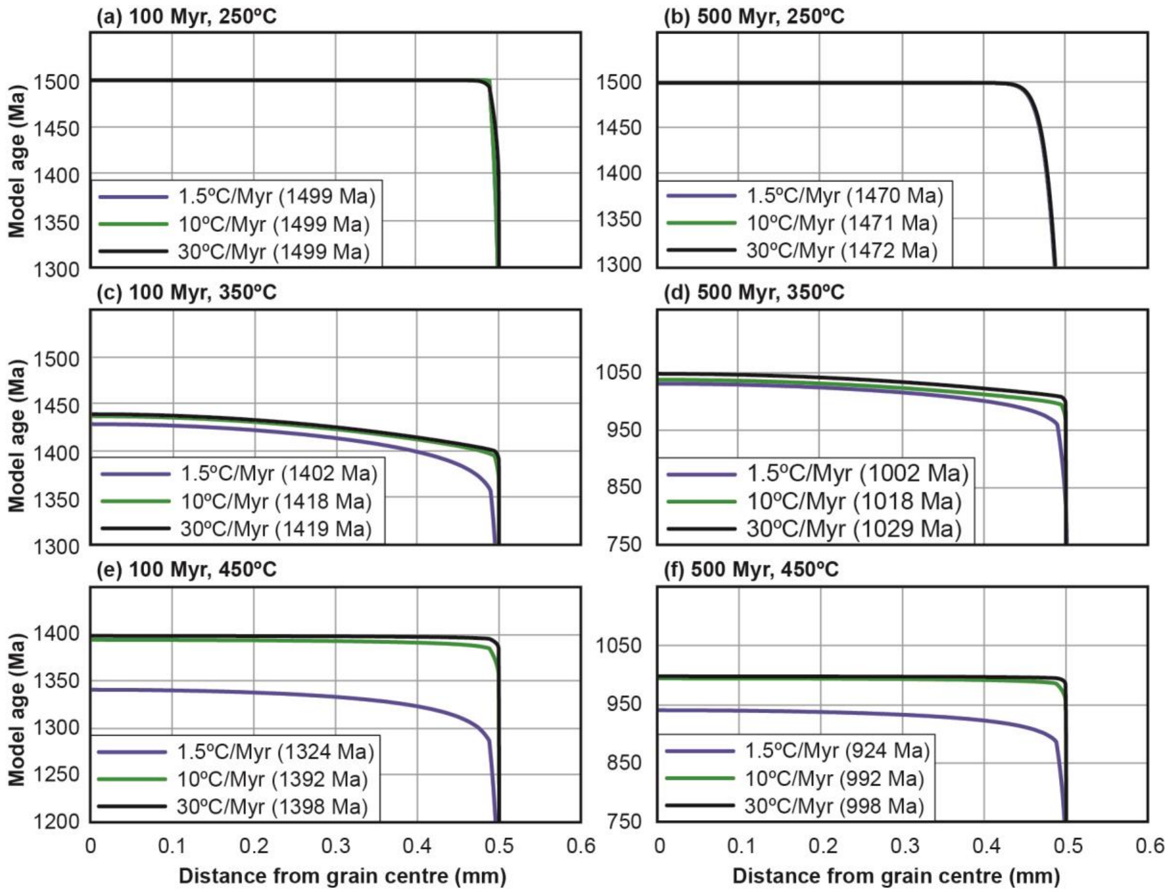

Fig. 5: Modelled core-to-rim $^{40}Ar/^{39}Ar$ age profiles for 0.5 mm-radius biotite that remained at temperatures of 250°C, 350°C or 450°C for 100 Myr or 500 Myr, then cooled at rates of 1.5°C/Myr, 10°C/Myr or 30°C/Myr. All models were run with an initial pressure of 0.7 GPa, followed by decompression that occurred simultaneously with cooling. Models were run from an arbitrary starting time of 1500 Ma; see text for details. Model bulk ages are shown in parentheses for each cooling rate.

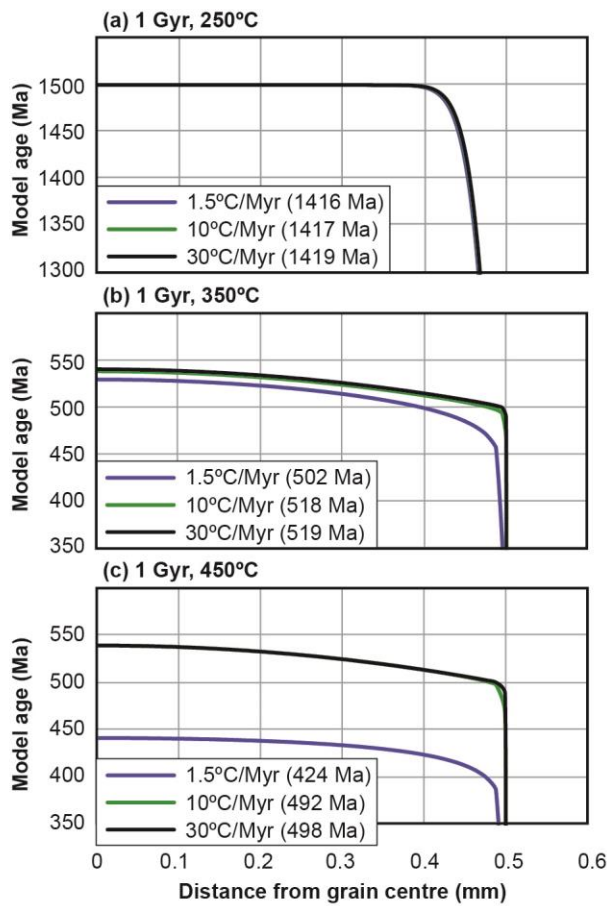

Fig. 6: Modelled core-to-rim $^{40}Ar/^{39}Ar$ age profiles for 0.5 mm-radius biotite that remained at temperatures of 250°C, 350°C or 450°C for 1 Gyr, then cooled at rates of 1.5°C/Myr, 10°C/Myr or 30°C/Myr. All models were run with an initial pressure of 0.7 GPa, followed by decompression that occurred simultaneously with cooling. Models were run from an arbitrary starting time of 1500 Ma; see text for details. Model bulk ages are shown in parentheses for each cooling rate.